ORIGINAL PAPER

Physical model experiment and numerical analysis on innovative gob-side entry retaining with thick and hard roofs

Xiaoming Sun [1,2] · Chengwei Zhao [1,2] · Gan Li [1,2] · Bo Zhang [1,2] · Junwei Wang [1,2] · Feng Cai [3]

Abstract

Gob-side entry retaining is a common method in underground coal mining. Conventional gob-side entry retaining (CGER) always causes stress concentration and large deformation around roadways under the condition of thick and hard sandstone roofs. Thus, an innovative method of no pillar gob-side entry retaining (NPGER) in longwall mining is proposed in this paper. First, a physical model was established to explore the mechanism of the new method. The modeling results indicate that the progressive caving of the strata in the middle of the stope is consistent with CGER. The major difference between NPGER and CGER is that CGER collapsed with a structure of a long arm beam, but NPGER collapsed with a structure of a short arm beam near the roadway. In the end, a new roadway with a gangue rib was formed when the immediate roof and main roof slipped along the pre-cutting plane. Subsequently, the numerical simulation software Universal Distinct Element Code (UDEC) was adopted to establish the numerical model of the 8501 working face in Tangshangou coal mine. The NPGER process is simulated. The evolution of the roof structure and stress characteristics were clearly demonstrated. The results showed that the roof structure noticeably changed from a long beam to a short beam after roof fracturing. The retained roadway was under low stress conditions, and the stress was transferred to the deep rock. In the end, the NPGER method was applied in the field, and the results showed that the retained roadway could meet the requirements of the next working face, which may provide guidance for longwall mining with thick and hard roofs.

Keywords Physical model experiment · Numerical simulation · Conventional gob-side entry retaining · No pillar gob-side entry retaining · Roof structure · Short arm beam

Introduction

Gob-side entry retaining is a common mining method in coal mining. In the conventional gob-side entry retaining (CGER) method, the entry of the current mining working face will be retained to be reused for the next working face by constructing

✉ Xiaoming Sun
  108830@cumtb.edu.cn

1   State Key Laboratory for Geomechanics & Deep Underground Engineering, China University of Mining & Technology, Beijing 100083, China

2   School of Mechanics and Civil Engineering, China University of Mining & Technology, Beijing 100083, China

3   Centre for Technology Management, China National Coal Group CO., Ltd., Beijing 100120, China

an artificial wall along the gob side. This method not only reduces the work of excavating roadways but also increases coal-recovery rates. Therefore, CGER is an efficient technique (Luan et al. 2018; Li et al. 2018; He et al. 2005; Zhang et al. 2012; Gong et al. 2018). However, not all geological conditions are suitable for CGER (Deng and Wang 2014; Zhang et al. 2014). CGER is usually suitable for roofs that easily collapse (Luo 2012). Due to the problem of roadway stress concentration and large deformation with thick hard sandstone roofs (Wu et al. 1997; Xue et al. 2013), the following two phenomena easily occur. First, the thick sandstone roof above the working face forms a large hanging roof, which leads to an increase in vertical stress and lateral stress in the rock surrounding the roadway. Second, when the elastic energy of a high-strength roof reaches the maximum bearing capacity of the surrounding rock, the energy is suddenly released and results in dynamic disasters such as rock bursts (Lu et al. 2015; Zhao et al. 2017; Li et al. 2017).

🖄 Springer

Much research has been done on CGER under the condition of a thick sandstone roof, which can be divided into two aspects. First, many scholars control the stress and deformation of the surrounding rocks by adjusting the strength of the backfill. Tan et al. (2015) proposed a new rigid-flexible composite support structure that can be effectively applied to gob-side entry in thin coal seam mining. Based on the deformation and control theoretical model of the coal-backfill-gangue support system, Ning et al. (2018) proposed a new composite material for CGER that can guarantee the stability of the surrounding rock in field applications. Xue et al. (2013) studied the width of the filling wall of CGER using FLAC 2D software and concluded that the stress concentration on the outer side of the filling wall was significantly greater than that on the inner side. In conclusion, the filling wall can control the deformation of the roof to some extent. However, the control is severely limited by the supporting materials and supporting equipment. Second, the common method currently is to control the mechanical behavior of the roof by changing the mechanical properties of the roof, such as pre-splitting blasting and hydraulic fracturing. Zhang et al. (2018) applied shallow hole blasting to CGER, and the mechanism was also explored by field tests and numerical simulation. The results showed that shallow hole blasting can effectively cut off the stress of the roof. Based on field measured data and numerical models, Yan et al. (2018) studied the relationship between the width of the filling body beside roadways and cutting resistance. Combined with numerical analysis of FLAC 3D, Zhang et al. (2017) proposed roof optimization technology with the core of the cutting roof and found that cutting roof technology can effectively reduce the deformation along the roadway caused by the rotation and subsidence of the cantilever beam. Han et al. (2015) established a mechanical model of a lateral cantilever beam, and the results showed that the length of the lateral roof cantilever beam along the roadway is the main factor affecting the stress concentration and deformation of the rock surrounding the roadway. Based on the Universal Distinct Element Code (UDEC) numerical simulation, Han also obtained the optimal cantilever beam length along the lateral roof of the gob-side entry and verified it in a field test. For the problem of CGER with hard roofs, Liu et al. (2018) proposed technology combined with support and roof cutting and achieved good control effects in field tests. Huang et al. (2018) established a mechanical model for the optimal fracture location of a cantilever beam along the gob-side entry and summarized the reasonable criterion of the fracture location for directional hydraulic fracturing with a hard roof, which provided a reference for a reasonable cutting location.

A filling wall or coal pillar is usually required in the traditional roof cutting technology of CGER. There are two shortcomings: first, the filling wall increases the cost of roadway support; second, coal pillars increase the waste of resources.

He et al. (2007, 2017b), He and Guo (2011), Sun et al. (2018b), Wang et al. (Wang et al. 2018a, b, c; Wang et al. 2020a, b), Yang et al. (2019), and Zhang et al. (2011) proposed the technology of a no pillar gob-side entry retaining (NPGER) roadway by cutting the roof connected to the gob with the entry. The process is as follows: the pre-splitting blasting is carried out along the gob side inclined to the side of the working face, and the blasting cutting plane parallel to the working face strike is generated along the gob-side entry roof. Due to the mining stress, the roof slides down along the blasting cutting plane, and finally, the roadway is formed (see Fig. 1). Based on field engineering and numerical analysis of FLAC 3D, Sun et al. (2014) studied the parameters of NPGER and pointed out that the cutting plane must deflect a certain angle to the gob to effectively cut off the roof stress. Based on numerical simulation theory, He et al. (2017a) compared the roof stress of NPGER with that of the conventional roadway and concluded that the vertical stress of the roof can be reduced along the no pillar gob-side entry, especially in the area affected by stress. Zhang et al. (2016) proposed the combined cutting roof scheme; that is, the roadway support and the roadside support should be strengthened, and the principle of upper pressure and lower support should be used to effectively cut the lateral roof to form a complete roadway. He et al. (2018) analyzed three kinds of roadway retaining methods from the surrounding rock stress: no pillar roadway, small pillar roadway, and large pillar roadway. The results showed that the stress concentration is smallest in no pillar roadway. In addition, Tao et al. (2018), Gao et al. (2017), Wang et al. (2020a, b), and Yang et al. (2020) also investigated the technology of NPGER in detail and discussed the parameters of roof cutting and support techniques.

The above research on NPGER at home and abroad mainly focused on theoretical analysis, numerical simulation, and field tests. However, it was difficult to consider all mechanical properties in the theoretical model (Sitharam and Latha 2002). Many scholars used FLAC 3D, the continuum method software, to investigate NPGER, and it is difficult to describe the caving processes. The UDEC, as the representative discontinuum method software, has been widely used for underground engineering because it is capable of capturing large displacements, caving, and rotations (Gao et al. 2015; Bai et al. 2016). Physical model testing is also a powerful method to investigate the stability and failure of geotechnical engineering structures. However, Meguid et al. (2008) emphasized that full-scale experiments are difficult to operate and that small-scale tests are limited by the model size, and in situ stresses are not realistically simulated, so many reduced-scale model tests have been conducted to investigate the failure mechanism of underground engineering (Ghabraie et al. 2015; Kang et al. 2018; Sun et al. 2017, Sun et al. 2018a; Tian et al. 2018; Wang et al. 2014; Wang et al. 2017; Xie et al. 2020; Zhao et al. 2019). Due to the complexity of

Fig. 1 Conventional gob-side entry retaining and no pillar gob-side entry retaining model. **a** Conventional gob-entry entry retaining. **b** Conventional roof cutting gob-entry entry retaining. **c** No pillar gob-entry entry retaining

(a) Conventional gob-entry entry retaining

(b) Conventional roof cutting gob-entry entry retaining

(c) No pillar gob-entry entry retaining
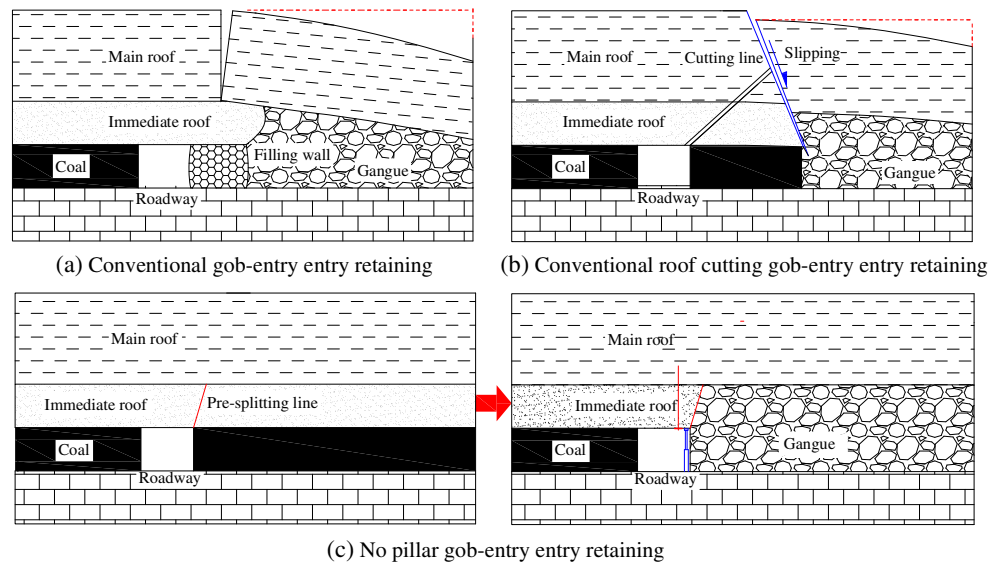
geological conditions, few scholars have investigated the mechanism of the NPGER with thick and hard roofs by the methods of physical model test and distinct element analysis.

In this paper, to obtain a better understanding of the mechanism of NPGER, a reduced-scale physical model experiment was first conducted based on the background of the 8501 working face in Tangshangou mine. The mechanisms of CGER and NPGER were analyzed from the caving processes and structures of the overlying strata. Then, numerical models with UDEC were built to investigate the mechanism of NPGER from the caving processes, roof structure, and stress distribution. Finally, the innovative NPGER method was successfully applied to the 8501 working face of Tangshangou mine.

Physical model experiment

Engineering background

Tangshangou coal mine is located in Datong city in China's Shanxi Province (Fig. 2). The minable coal seams are No. 8 and No. 12. The No. 8 coal seam belongs to a Mesozoic Jurassic Formation, and the occurrence conditions are stable. The dip angle of the No. 8 coal seam is 1°~3°, and the thickness is 1.5~2.3 m. The 8501 working face is located at a depth of approximately 175.0 m and has a height of 2.0 m. The width of the longwall is 115.0 m, and its length is 417.0 m (Fig. 3). The 8501 working face is overlain by an immediate 4.0-m strong medium-coarse sandstone. Above that is a main roof of a 9.0-m strong fine sandstone. The 8501 ventilation roadway, with a height of 2.5 m and length of 3.8 m, is the test roadway for roof cutting. The roof pre-cutting height is 6.0 m,

and the angle is 20 degrees. Figure 4 shows the thickness of the coal seam as well as some important stratum.

Physical similarity parameters

To master the rock mechanics properties of some important geotechnical parameters of the roadway for physical model experiments, rock samples are obtained from the roadway roof and floor of the 8501 working face. The lithology of the coal seam as well as some important geotechnical parameters is obtained from laboratory physical parameters, and Table 1 shows the theoretical similarity parameters.

Physical model experiments usually need to transform the actual geotechnical engineering environment to the experimental environment through a certain proportion. The corresponding points of the physical model and field model are similar in some movements, such as the velocity, acceleration, time, and strain. However, it is difficult to guarantee that all movements are similar. Therefore, some important similarity constants are selected as follows:

$$\begin{cases} C_L = \dfrac{L_p}{L_m} \\ C_t = \dfrac{t_p}{t_m} \\ C_E = \dfrac{E_p}{E_m} \\ C_\gamma = \dfrac{\gamma_p}{\gamma_m} \\ C_\sigma = \dfrac{\sigma_p}{\sigma_m} \end{cases} \tag{1}$$

where C_L is the geometric similarity constant, C_t is the time similarity constant, C_E is the elastic modulus similarity

Fig. 2 Location of the
Tangshangou coal mine, Shanxi,
China

Tangshangou
coal mine
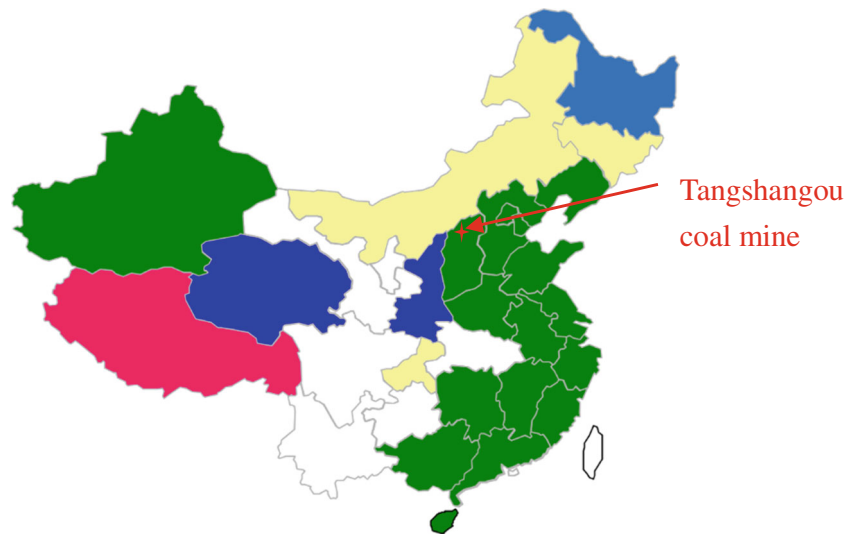
constant, C_γ is the body force similarity constant, and C_σ is the stress similarity constant.

In addition, the model should meet the differential equations of equilibrium, so the similarity constants should meet the following requirement:

$$\frac{C_\sigma}{C_L} = C_\gamma \tag{2}$$

In fact, it is difficult to find a kind of material to meet all the requirements that are mentioned above. Therefore, it is enough to make the key physical similarity constant meet the requirements. The physical model of the material is mainly composed of aggregate and cement. The mechanical properties of different mixture ratios of aggregate and cement vary greatly. The aggregate has an important effect on the properties of similar materials. Fine sand is selected as the aggregate and accounts for a large proportion in this study. The mechanical parameters of similar materials are determined by the

cement. According to the actual coal and rock mechanics properties, lime and gypsum are chosen as the cement in this study. To meet the laboratory requirements of the proportion and rock layer scheme, a series of laboratory experiments were performed to accurately select and calculate the proportional parameters. Table 2 shows the rock layer scheme and the proportional parameters of some important rock layers in this physical model experiment.

Physical model establishment

Based on the dimensions of the physical model experiment platform (length × width × height = 1800 mm ×
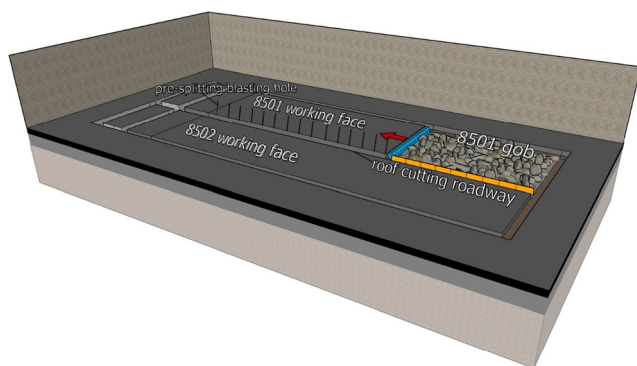

Fig. 3 Layout of panel and 8501 roadway at the study site. The study site was the 8501 roadway which was cutting the roof to form the no pillar gob-side entry

Lithology	Lithological log	Thickness (m)
Gritstone		20.5
Fine sandstone		48.0
Siltstone		4.0
Carbonaceous		1.7
Coal seam		0.3
Fine sandstone		9.0
Medium coarse		4.0
No. 8 coal seam		2.0
Siltstone		15.0

Fig. 4 Lithology of the study site

Table 1 Parameters of each layer in the experimental model

Layer number	Lithology	Thickness		Compression strength		Bulk density	
		Prototype (m)	Model (mm)	Prototype (MPa)	Model (MPa)	Prototype (g/cm^3)	Model (g/cm^3)
7	Coarse sandstone	20.5	205	51.21	0.320	2.31	1.44
6	Fine sandstone	48.0	480	60.13	0.376	2.68	1.67
5	Siltstone	4.0	40	57.02	0.356	2.65	1.66
4	Carbonaceous mudstone	1.7	17	12.15	0.076	2.35	1.47
3	Coal line	0.3	3	12.34	0.077	1.43	0.89
2	Fine sandstone	9.0	90	65.14	0.407	2.37	1.48
1	Medium-coarse sandstone	4.0	40	62.52	0.391	2.31	1.44
0	No. 8 coal seam	2.0	20.0	12.31	0.077	1.43	0.89
− 1	Siltstone	15.0	150.0	56.06	0.350	2.40	1.50

160 mm × 1300 mm), the physical model was established with the geometric similarity constant of 100, the stress similarity constant of 160, and the body force similarity constant of 1.6 to simulate the actual rock mass dimension of 180 m × 16 m × 104.5 m. The horizontal displacement was constrained along the lateral boundaries of the model, and the vertical and horizontal displacements were fixed at the bottom boundary. To simulate the in situ rock stress of the coal seam at a depth of 175 m, vertical stress was applied to the upper boundary to simulate the remaining overburden stress of 70.5 m. According to the size of the model and a predetermined ration, the bulk density of the overlying strata was 2500 kg/m³. The gravity of the overlying strata was 1.763 MPa. According to the calculated stress similarity constant, the actual overburden stress of the physical model was 11 kPa.

Experimental scheme

Monitoring approach

The cross intersect method was used to arrange the displacement measuring points in the overlying strata of the coal seam. Above coal seam no. 8, 9 rows of measuring points in the horizontal direction of the overlying strata were set up. The distance between the measuring points of each layer was 10 cm, and the first row of measuring points was 3 cm from the roof of the coal seam. In the vertical direction, the measuring points were arranged from the left side of the roadway. A total of 17 measuring points were arranged, and the column spacing was 10 cm. A total of 153 displacement measuring points were arranged to monitor the collapse and movement of the overlying strata, as shown in Fig. 5.

Table 2 Material usage of the model

| Layer number	Lithology	Layer thickness (cm)	Fine sand weight (kg)	Lime weight (kg)	Gypsum weight (kg)	Water weight (kg)
7	Coarse sandstone	20.5	90.30	6.80	4.50	7.10
6	Fine sandstone	48.0	208.08	14.88	14.88	16.56
5	Siltstone	4.0	17.62	1.10	1.10	1.38
4	Carbonaceous mudstone	1.7	7.49	0.56	0.37	0.59
3	Coal line	0.3	1.32	0.12	0.05	0.10
2	Fine sandstone	9.0	39.00	2.80	2.80	3.12
1	Medium-coarse sandstone	4.0	17.62	1.10	1.10	1.38
0	No. 8 coal seam	2.0	8.81	0.77	0.33	0.69
− 1	Siltstone	15.0	9.32	0.67	0.67	0.75
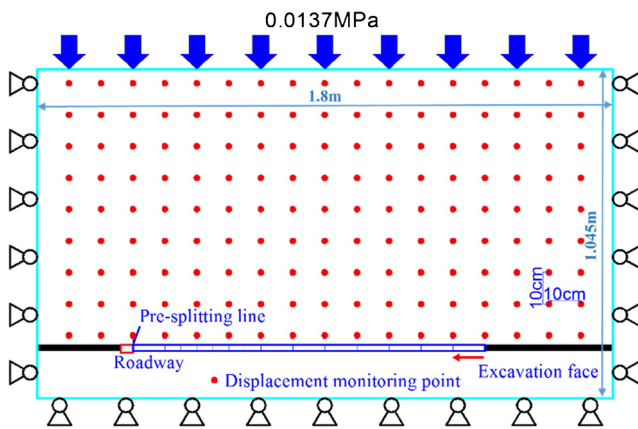
Fig. 5 Boundary condition applied

The MV-VDM small USB 3.0 interface high-speed industrial digital camera (Fig. 6) was used to measure the coordinate changes in the layout points to obtain the displacement of the overlying strata on the model. At the same time, the typical phenomenon of the overlying strata movement was recorded by a digital camera.

Excavation scheme

To obtain the temporal and spatial distribution characteristics of the working face inclined to collapse, the excavation was started along the boundary of the model with a distance of 400 mm from the boundary of the coal seam. The first 600 mm was excavated 100 mm each time, and the last 500 mm was excavated 50 mm each time. Before the upper basic sandstone broke, we waited 30 min after each excavation before continuing excavation. After the upper basic sandstone broke, we waited 5–10 min after each excavation. Before the coal seam was excavated, the time between the laptop and the high-speed camera was adjusted to the waiting time of the excavation. The time of starting excavation, stopping excavation, and rock collapse were recorded during the

Fig. 6 Layout of the monitoring equipment on the similar simulation model

experiment. A very thin iron sheet was set into the pre-splitting position during the laying process of physical model. The height of the iron sheet is consistent with that of the pre-splitting. After roadway excavation, the iron sheet was pulled out from the rock layers in the back of physical model to simulate the pre-splitting. The excavation method is manual excavation. The steel ruler was used to measure the excavation length, and then the saw blade was used for excavation with 160-mm thickness. After coal seam excavation, we observed, took pictures, and recorded the deformation value until the coal seam was mined out.

Numerical simulation

Physical model experiments can directly provide the deformation and caving characteristics of the overlying strata and the change in the lateral roof structure from a long arm beam to a short arm beam during roadway roof cutting. However, the deformation and caving are not sufficient to explain the NPGER. The discrete element software Universal Distinct Element Code (UDEC) based on Lagrangian theory is used to check the physical model and numerical model parameters to establish a model of NPGER and CGER. The mechanism of cutting the roadway roof with pressure relief will be further revealed during the change in lateral roof structure and roadway stress.

UDEC introduction

To obtain a deeper understanding of the failure mode and mechanism of roadway excavation and coal seam mining, UDEC (Itasca Cons 2014), a discrete element method, is suggested to be an effective numerical technique for simulating such physical model problems and analyzing the stability of underground excavations compared with the use of finite element modeling (Roest et al. 1990).

In UDEC, the rock mass is represented by discrete blocks and contacts. The blocks in UDEC can be regarded as rigid and deformed, and they are allowed to move, rotate, and deform. The contacts are between these blocks, and they can be opened and slipped with each other. The geometrical model can change largely through the use of a contact updating scheme. When the model is applied by load or the forces of neighboring blocks, the motion of the blocks follows Newton's second law of motion.

The subsidence, fracture, and caving of overlying strata occur along the contacts through shear or tension, depending on the stress state of the contact surface. The contact surface stress is determined by the displacement of the contacts. In the normal direction of a contact, the stress-displacement relation is expressed as follows:

$$\Delta \sigma_n = -k_n \Delta u \qquad (3)$$

where $\Delta \sigma_n$, Δu, and k_n are the normal stress change, normal displacement change, and normal stiffness of a contact, respectively.

In the shear direction, the shear stress is determined by the contact microproperties, cohesion (c), and friction (φ). If

$$|\sigma_s| \leq c + \sigma_n \tan \varphi = \sigma_s^{max} \qquad (4)$$

then,

$$\Delta \sigma_s = -k_s \Delta u_s^e \qquad (5)$$

If

$$|\sigma_s| \geq \sigma_s^{max} \qquad (6)$$

Then,

$$\sigma_s = \text{sign}\left(\Delta u_s^e\right) \sigma_s^{max} \qquad (7)$$

where Δu_s^e is the elastic component of the incremental shear displacement and Δu_s is the total incremental shear displacement.

According to these equations, the incremental stresses are calculated at each time step and added to the existing stresses. The status of the contacts is determined by the Mohr-Coulomb failure criterion.

Numerical simulation scheme

The numerical model was constructed by using rectangular blocks, as shown in Fig. 7. The dimensions of the numerical model are 180 m long and 104.5 m high. First, the model was divided by bedding planes into nine rectangular blocks with nine different lithologies. Then, the nine rectangular blocks were discretized into small rectangular blocks with preexisting discontinuities, including bedding planes and cross joints. In the bottom and top of the model, the siltstone, gritstone, and part of the fine sandstone were discretized into rectangular blocks with an average edge length of 8 m × 4 m. The remainder of the model was assigned rectangular blocks with an average edge length of 1 m × 0.5 m, which is sufficiently fine to simulate roof caving and stress. Compared with the CGER model, a pre-cutting plane was added at the upper right corner of the roadway in the NPGER model. To obtain a better cutting effect, a very thin parallelogram block with a height of 6 m and an angle of 20° was designed to simulate the pre-cutting plane.

According to data obtained from the in situ stress measurements, the horizontal stress was parallel to the longwall advance direction with a value of 4.375 MPa, and the vertical stress was perpendicular to the longwall advance direction with a value of 4.375 MPa. The displacements of the left and right boundaries were fixed in the horizontal direction. The displacement of the bottom boundary was fixed in the vertical direction. A force of 1.763 MPa was applied on the top model boundary equivalent to the overburden weight. Based on iterative back-analysis of the numerical result and the laboratory UCS test, the normal stiffness of 85 GPa/m and shear stiffness of 34 GPa/m were set to represent the deformability of the coal seam contacts. Other mechanical parameters of the rock mass are shown in Tables 3 and 4.

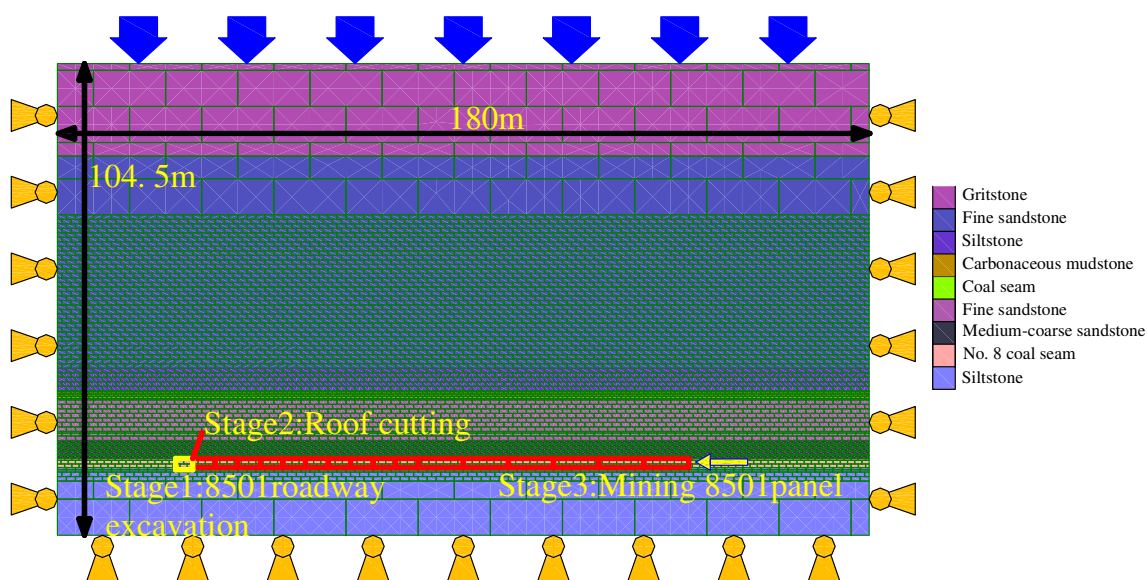The realization of CGER and NPGER can be summarized as follows:

Fig. 7 Numerical simulation experimental model

Table 3 The main physical and mechanical parameters of layers set in numerical model

Lithology	Thickness (m)	Density (kg/m^3)	Bulk modulus (GPa)	Shear modulus (GPa)
Siltstone	15	2400	3.20	2.5
No. 8 coal seam	2	1420	1.20	0.8
Medium-coarse sandstone	4	2300	4.32	2.8
Fine sandstone	9	2368	4.48	3.0
Coal seam	0.3	1420	1.20	0.8
Carbonaceous sandstone	1.7	2350	1.28	0.9
Siltstone	4	2600	3.20	2.5
Fine sandstone	48	2670	4.48	3.0
Gritstone	20.5	2300	4.32	2.8

(1) Stress equilibrium state: both the CGER model and NPGER model should be run to equilibrium first to generate the in situ stress before roadway excavation.

(2) Roadway excavation: after the pre-mining stress is assigned, the 8501 roadway was excavated by deleting the blocks in both the CGER model and the NPGER model. Rock bolts and the steel straps were installed immediately after deletion of the blocks.

(3) Generation of the pre-cutting plane: the pre-cutting plane was only set in the NPGER model. In this stage, the pre-cutting plane was generated by deleting the parallelogram block. To increase comparability, the same steps were conducted to relieve stresses in both models.

(4) 8501 working face: to ensure realistic mining-induced stresses, the extraction of the 8501 working face was simulated by means of a stepwise excavation. The first 60 m comprised a total of six stages with each stage involving a 10 m advance from right to left in the model. In the last 50 m, a total of ten stages were run with each stage involving a 5 m advance from right to left in the model. For each stage, sufficient time steps were run to relieve stress and to allow the roof to cave.

## Mechanism of NPGER

Progressive caving of the strata

Coal mining in underground always causes the intense movement of overlying strata, such as bending, fracture, subsidence, and separation, which generates many fissures. As the mining face advanced, the fissures will experience the processes of initiation, propagation, and closure.

Figure 8 shows the process of excavating the coal seam step by step by physically and numerically simulating longwall mining. When the excavation face is advanced to 40 m, the first fracture occurred in 4.0-m-thick medium-coarse sandstone (immediate roof), and the bending and subsidence appeared in the immediate roof. The main roof of the 9.0-m-thick fine sandstone overlying immediate roof is exposed due to the separation between the main roof and immediate roof. In this stage, many vertical fissures and separation fissures generated. When the excavation face advanced to 50 m, the fracture occurred in the main roof, accompanied by bending, subsidence, and separation. Therefore, it was considered that the initial caving interval of the main roof is 50 m. A

Table 4 The main joint parameters of layers set in numerical model

Lithology	Normal stiffness (GPa)	Shear stiffness (GPa)	Cohesion (MPa)	Internal friction angle (°)	Tensile strength (MPa)
Siltstone	85	34	2.40	28	1.28
No. 8 coal seam	28	11	0.96	20	0.50
Medium-coarse sandstone	107	42	1.92	23	0.80
Fine sandstone	106	42	2.88	25	1.28
Coal seam	28	11	0.96	20	0.50
Carbonaceous sandstone	40	21	1.28	25	0.64
Siltstone	85	34	2.40	28	1.28
Fine sandstone	106	42	2.88	25	1.30
Gritstone	150	60	3.20	28	1.80

Fig. 8 Progressive caving of the strata and no pillar gob-side entry retaining forming. **a** Immediate roof caving. **b** Main roof caving. **c** The overlying strata bending and separating. **d** Roof periodic rupture. **e** Lateral roof hanging. **f** Roadway forming with lateral roof collapse

(a) Immediate roof caving

(b) Main roof caving

(c) The overlying strata bending and separating

(d) Roof periodic rupture

(e) Lateral roof hanging

(f) Roadway forming with lateral roof collapse
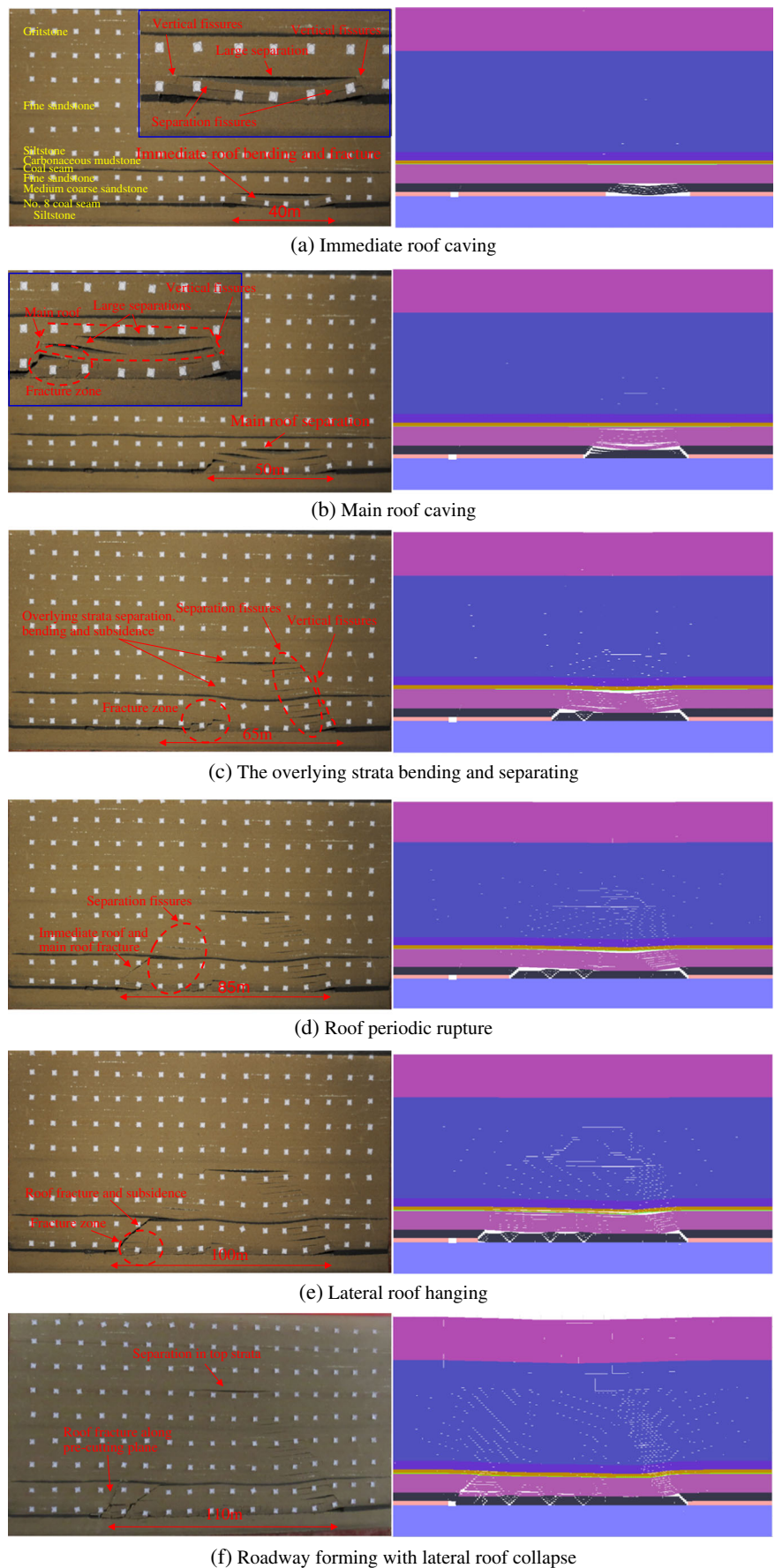
fracture zone was formed due to the breaking down of the immediate roof. When the excavation face advanced to 65 m, 0.3-m-thick coal seam line, 1.7-m-thick carbonaceous mudstone, and 4.0-m-thick siltstone gradually bent and sank layer by layer. What's more, 48.0-m-thick fine sandstone was gradually exposed due to the separation. Many separation fissures and vertical fissures occurred due to the subsidence of strata. When the excavation advanced to 85 m, the immediate roof and main roof showed integral fracture and subsidence, accompanied by separation fissures occurring in the overlying roof. The complete fracture and subsidence occurred when the excavation face advanced to 100 m, and the separation phenomenon appeared between carbonaceous mudstone and overlying siltstone. Also, the roof was in the state of a long cantilever. As the excavation face advanced to 110 m, the immediate roof and main roof broke and slipped along the pre-cutting plane, bending subsidence developed to the top strata. The separations of lower strata gradually closed. The collapse of the roof filled beside the roadway and formed the support structure.

The characteristics of rock strata movement of NPGER in mining stope can be summarized as follows:

(1)   The collapse of rock strata of NPGER in the middle of the mining stope is consistent with that of CGER, both of which show the characteristics of progressive upward development of strata bending, sinking, and separation.

(2)   In the upward and gradual development of rock strata movement, the rock strata above the main roof, such as the soft coal line, carbonaceous mudstone, and siltstone, mostly bent, sank, and separated in an instant. There is no obvious hanging phenomenon in the process of strata movement. However, the movement of thick and hard sandstone is characterized by obvious long-distance suspension, just like a beam (Gao et al. 2014). The beam will show a one-time fracture when the vertical stress is dominant.
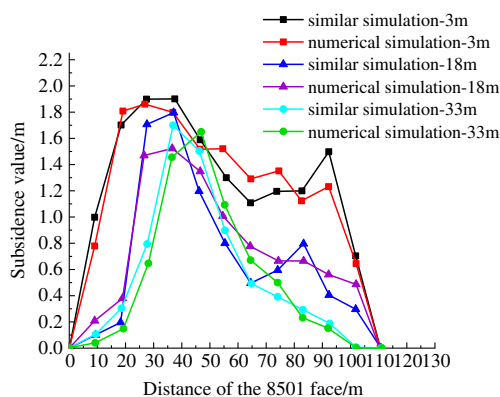
(3)   When the excavation face is close to the roof of the roadway, the lateral roof caving characteristics of NPGER are obviously inconsistent with CGER due to the existence of pre-cutting plane. There is little time for the lateral thick sandstone roof to hang, and it breaks down along the pre-cutting plane in a short time. Also, the immediate roof and main roof showed the characteristics of one-time overall breaking.

Three measuring lines were laid out at 3 m, 18 m, and 33 m above the coal seam roof, and the results are plotted in Fig. 9. The subsidence curves of the rock layers showed the "V shape" deformation of mining to 110 m. The subsidence curve of the numerical simulation was consistent with that of the physical model, and the numerical simulation can accurately simulate the process of physical model excavation.

Figure 10 shows the failure crack percentage during the excavation process. The failure crack percentage, which is the ratio of failure joint length to total joint length, includes shear crack failure and tensile crack failure. When the excavation face continued increasing, the tensile failure and shear failure cracks greatly increased, especially the tensile failure cracks. After the first strata collapsed after a 50 m advance of the excavation face, failure cracks quickly occurred in the subsequent excavation. Figure 11 shows the displacement vectors during the excavation process. The displacement showed that both the CGER and NPGER had similar deformation processes in the first 100 m of excavation. In the final excavation stage, the deformation area of NPGER was larger than that of CGER due to the overburden strata slipping to form the roadway.

Structure of the short arm beam and formation of the roadway

When the excavation face advanced 100 m, the main roof and the immediate roof began to fracture because of subsidence
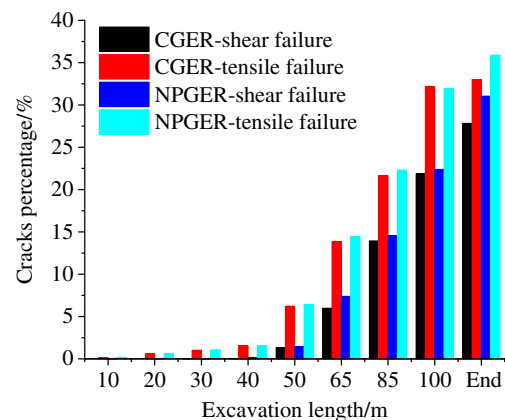
Fig. 9 Collapse curve of overlying strata in similar and numerical model experiments

Fig. 10 The failure crack percentage of numerical model during the excavation

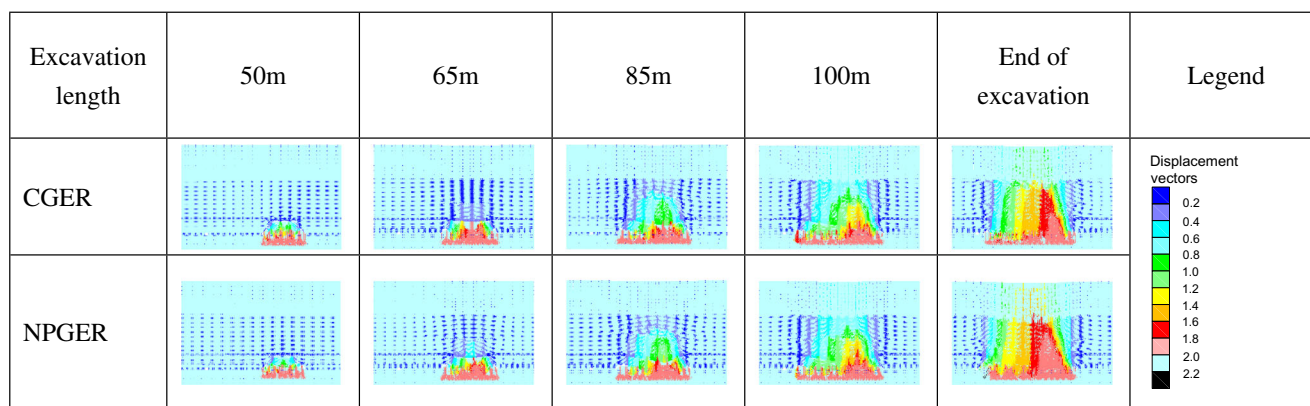| Excavation length	50m	65m	85m	100m	End of excavation	Legend
CGER						Displacement vectors 0.2 0.4 0.6 0.8 1.0 1.2 1.4 1.6 1.8 2.0 2.2
NPGER						

Fig. 11 Displacement vectors of rock blocks during the excavation in numerical model experiments

and rotation of the overlying strata in the mined-out area. The fracture extended from the main roof to the immediate roof. Due to the high strength of the main roof and the immediate roof, different lengths of long cantilever roofs were formed along the gob side (Fig. 12b). As shown in Fig. 12b, when the excavation face advanced 105 m, the cantilever ruptured suddenly under the disturbance of the mining stress. When the excavation face advanced 110 m, the coal seam was mined out, and the roof began to fracture along the pre-cutting plane. A 4.0-m-thick immediate roof of medium-coarse sandstone broke along the pre-cutting plane and formed a wedge-shaped short arm beam. The 9.0-m-thick main roof of fine sandstone also formed a short arm beam along the cutting plane. There was no obvious separation between the immediate roof and the main roof. The overburden strata basically experienced extension fracture along the cutting plane, and finally, the immediate roof and the main roof formed the overall structure of the short arm beam (Fig. 12d, e).

The immediate roof and the main roof fracture slipped along the cutting plane together in a timely manner under

the stress of gravity and mining. The collapsed roof could basically fill the roadside after crushing and swelling because of the rotation and subsidence of the overlying strata, forming the roadway rib and supporting the roadway roof to a certain extent. Finally, NPGER with a short arm beam structure was formed (Fig. 12d, e).

Stress changes

In field tests, a pre-cutting plane is usually formed on the roadside roof parallel to the roadway strike by directional blasting after roadway excavation. To simulate the process of the pre-cutting plane in this numerical simulation, blocks were deleted. Figure 13 a and b show the excavation of the 8501 roadway and the excavation of the pre-cutting plane.

After the excavation of the roadway, the stress was symmetrically distributed at the boundaries of the roadway, and stress was relieved in the roof and floor of the roadway. Mining of the 8501 roadway altered the stress conditions, resulting in stress concentration at the two sides of the

Fig. 12 Formation process of short arm beam and no pillar roadway in thick sandstone roof. **a** Lateral roof hanging. **b** Long arm beam. **c** Fracturing along the pre-cutting plane. **d** Short arm beam and roadway forming. **e** Roadway forming in numerical simulation

(a) Lateral roof hanging   (b) Long arm beam   (c) Fracturing along the pre-cutting plane

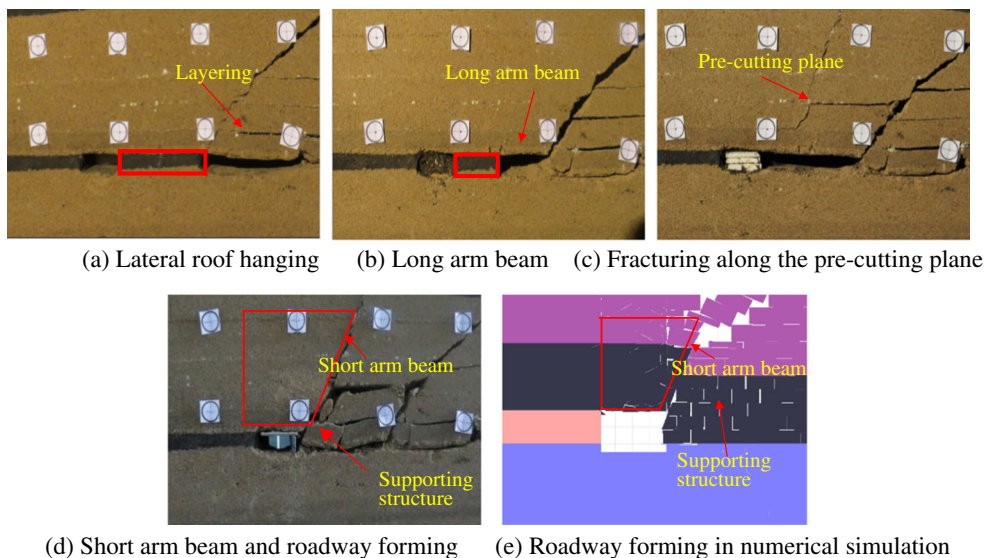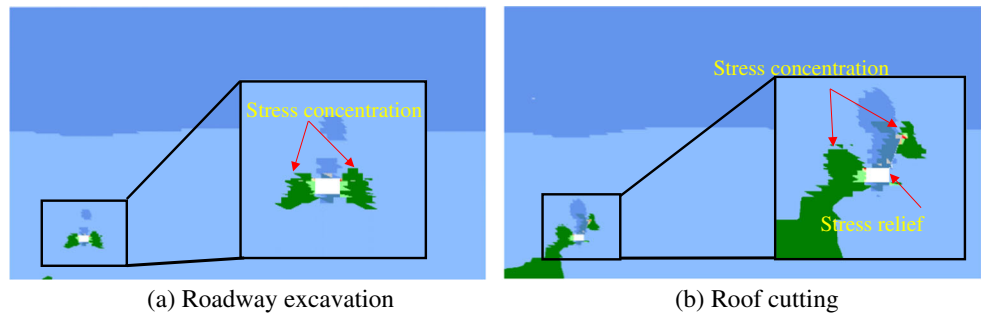(d) Short arm beam and roadway forming   (e) Roadway forming in numerical simulation

Fig. 13 Excavation of roadway and joint-cutting. **a** Roadway excavation. **b** Roof cutting

(a) Roadway excavation

(b) Roof cutting

roadway, especially at the shoulder of the two sides. The maximum concentration coefficient was 1.5. On the basis of roadway excavation, a cutting plane was formed by deleting the

preset blocks. The characteristics of asymmetric distribution around the roadway were present. Deleting the preset blocks altered the stress conditions again, resulting in stress

Fig. 14 Simulated vertical stress distribution with longwall face advance. **a** 40 m. **b** 50 m. **c** 65 m. **d** 85 m. **e** 100 m. **f** CGER. **g** NPGER

(a) 40 m

(b) 50 m

(c) 65 m

(d) 85 m

(e) 100 m

(f) CGER

(g) NPGER
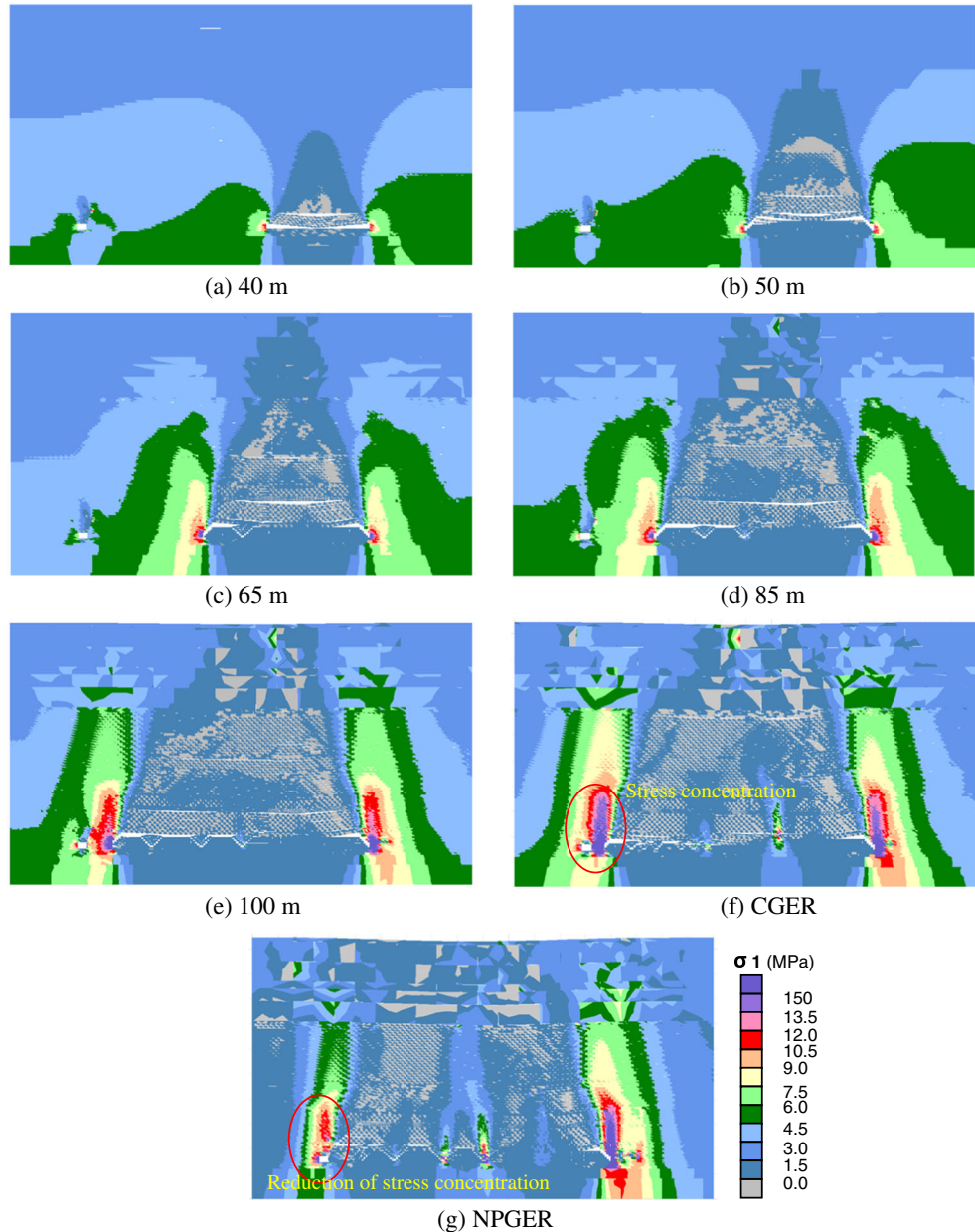
concentration on the left side of the roadway and the end of the cutting plane line and relief in the roof and the right side of the roadway, as shown in Fig. 13 a and b.

Knowledge of the stress change is very important in understanding the caving process of the gob and the difference between CGER and NPGER. The vertical stress distribution at different mining stages is shown in Fig. 14. The extraction of the coal led to stress concentration around the unmined coal. The vertical stress in the immediate roof and floor was relieved as the coal mining advanced. When the face advanced to 40 m, the immediate roof collapsed, resulting in a closure of the mined area. The main roof began to collapse when the face advanced to 50 m. The vertical stress continued to increase around the rear and front of the coal after the overlying strata collapsed.

When the face advanced to 100 m, the vertical stress around the roadway increased sharply (Fig. 15). The maximum stress on the right side of the roadway was 9 MPa, and the maximum stress on the left side was 7.2 MPa. For CGER, the maximum stress on the right side was 12 MPa, and the maximum stress on the left side was 10 MPa. However, there was an obvious stress reduction zone after the immediate roof and main roof slipped along the cutting plane (Fig. 14g). The stress concentration was eliminated, and stress was transferred to the surrounding rock of the deep roof.

The modeled vertical stress changes were plotted in detail at selected monitoring points with face advancement. The monitored vertical stress at 4 points is shown in Fig. 15. In the roof and floor of the 8501 roadway, the vertical stress dropped sharply after the coal seam was mined out (P1, P2). The vertical stress in the right wall of the roadway was eliminated. Figure 15 b shows the vertical stress under the condition of CGER. The vertical stress of all monitoring points, especially monitoring point P4 located in the middle of the pillar between the 8501 goaf and the 8501 roadway, increased significantly after mining out of the coal seam, indicating that the surrounding rock, especially the pillar, carried too much stress to guarantee the stability of the roadway.

Engineering application

A field test was conducted in the 8501 ventilation roadway with a length of 417 m. The cutting plane with a height of 6 m and an angle of 20° was designed to cut the roof by cumulative explosion technology. Before the cutting plane, the anchor cable support system was installed in the roadway to maintain the stability of the roadway, as shown in Fig. 16. As the working face was excavated, the pillar support system was installed

(a) No pillar gob-side entry retaining   (b) Conventional gob-side entry retaining
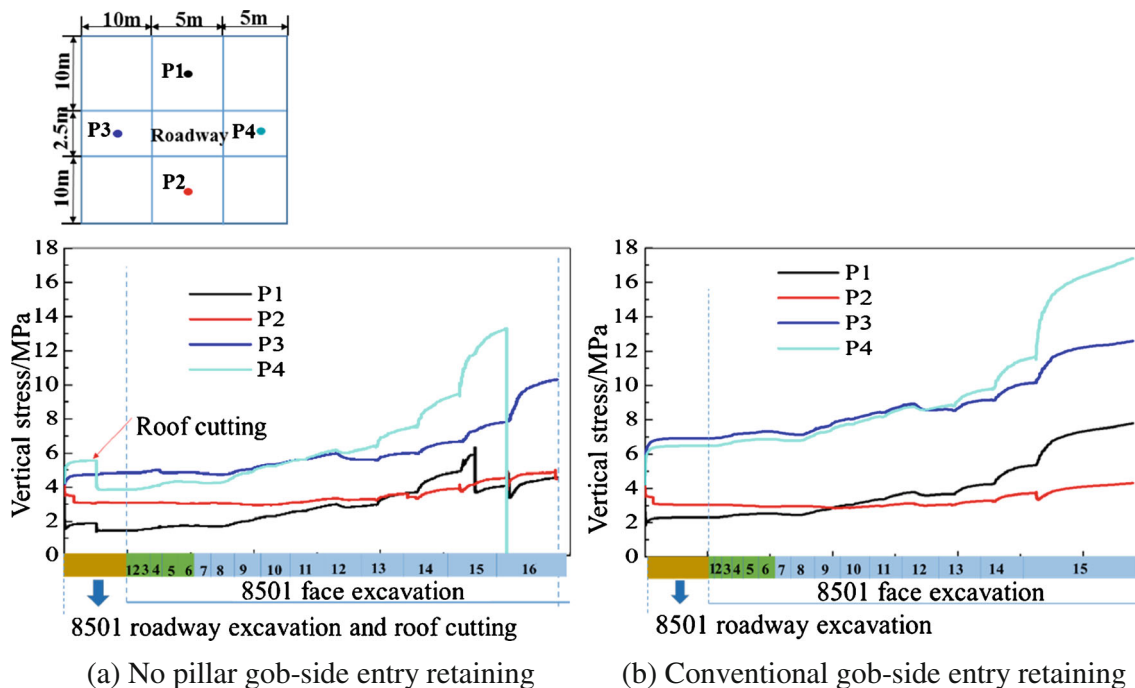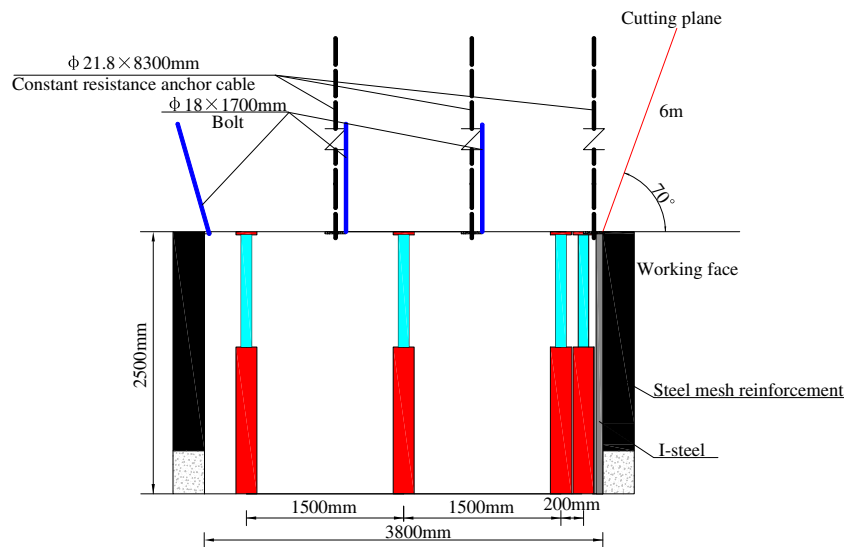
Fig. 15 Simulated vertical stress changes around the 8501 roadway under conventional gob-side entry retaining and no pillar gob-side entry retaining. **a** No pillar gob-side entry retaining. **b** Conventional gob-side entry retaining

Fig. 16 The support system in retained roadway

in the roadway to ensure the successful separation of the working face roof and roadway roof, and I-steel was installed along the roadway side to prevent gangue, as shown in Fig. 16. In the end, as the roof bent, collapsed, and caved, the gangue rib gradually formed. Figure 17 shows the curves of the roof and rib convergence values monitored in the retained roadway. As the distance to the working face increased, the convergences were gradually stable. When the convergence was stable, the pillar supports were removed, as shown in Fig. 18b.

The field test results showed that the NPGER technique not only eliminated the influence of the working face roof on the roadway but also formed a new roadway to be used in the next working face. Additionally, due to the anchor cable support system and pillar support system, the overall section shape of the roadway is better, which can meet the usage requirements for the next working face. Figure 18 shows the effect of the retained roadway on site.
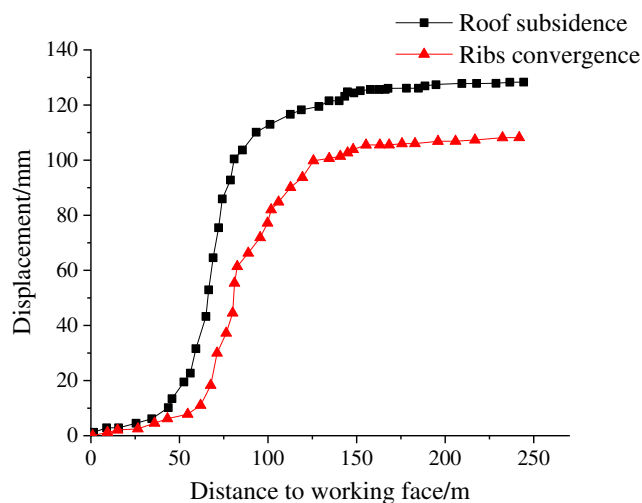

Fig. 17 The monitoring curve of roof subsidence and ribs convergence

Conclusions

In this paper, based on the field test of the 8501 ventilation roadway of Tangshangou coal mine in Datong city, a new gob-side entry retaining method was introduced in detail by physical model and numerical simulation experiments. The paper describing the new method mainly focuses on the progressive caving of the strata, the formation of a short arm beam structure and roadway, and the stress characteristics.

The results show that the progressive caving caused by extraction of the longwall panel, including immediate and main roof collapsing and overlying strata bending in the rock mass, had been successfully demonstrated in the physical model experiment and numerical simulation. The caving processes of CGER and NPGER were similar in the middle panel area. The caving of rock strata gradually develops upward, and the scope of the caving rock strata is limited at each caving. In the process of gradual upward development, the softer coal seam, sand and mudstone, and other rock layers are mostly inclined to bend, sink, and separate from the layers. However, the movement of thick and hard sandstone layers is mainly characterized by long-distance overhanging and single fracture.

Due to the existence of the cutting plane, the collapse characteristics of the lateral roof are obviously inconsistent with CGER when entering closely to the roadway. CGER collapsed with a long arm beam, and NPGER collapsed with a short arm beam. In the NPGER method, the roadway with a gangue rib formed with the immediate roof and main roof slipping along the cutting plane. Additionally, the gangue rib provided support for the roadway roof.

The numerical simulation indicated that NPGER could strongly release roadway pressure. The stress increased sharply in CGER, the maximum stress coefficient on the right side was 4, and the maximum stress concentration coefficient on

Fig. 18 The formed roadway in the 8501 working face

the left side was 2.7. In the NPGER method, the maximum stress concentration coefficient on the left side was 2.3. The engineering applications showed that the deformation of the rock surrounding the retained roadway is small and that the retained roadway could meet the requirements of the next working face. The application of the NPGER method in coal mines with thick and hard roofs is feasible.

References

Bai QS, Tu SH, Zhang C, Zhu DF (2016) Discrete element modeling of progressive failure in a wide coal roadway from water-rich roofs. Int J Coal Geol 167:215–229

Deng YH, Wang SQ (2014) Feasibility analysis of gob-side entry retaining on a working face in a steep coal seam. Int J Min Sci Technol 24(4):499–503

Gao F, Stead D, Coggan J (2014) Evaluation of coal longwall caving characteristics using an innovative UDEC Trigon approach. Comput Geotech 55:448–460

Gao FQ, Stead D, Kang HP (2015) Numerical simulation of squeezing failure in a coal mine roadway due to mining-induced stresses. Rock Mech and Rock Eng 48(4):1635–1645

Gao YB, Liu DQ, Zhang XY, He MC (2017) Analysis and optimization of entry stability in underground longwall mining. Sustainability 9(11):2079–2098

Ghabraie B, Ren G, Zhang XY, Smith J (2015) Physical modelling of subsidence from sequential extraction of partially overlapping longwall panels and study of substrata movement characteristics. Int J Coal Geol 140:71–83

Gong P, Ma ZG, Ni XY, Zhang RR (2018) An experimental investigation on the mechanical properties of gangue concrete as a roadside support body material for backfilling gob-side entry retaining. Adv Mater Sci Eng 2018:1–11

Han CL, Zhang N, Li BY, Si GY, Zheng XG (2015) Pressure relief and structure stability mechanism of hard roof for gob-side entry retaining. J Cent South Univ 22(11):4445–4455

He MC, Guo ZB (2011) Mechanical property and engineering application of anchor bolt with constant resistance and large deformation. Chin J Rock Mech Eng (China) 7:1297–1308

He MC, Xie HP, Peng SP (2005) Study on rock mechanics in deep mining engineering. China J Rock Mech Eng (China) 24(16): 2803–2813

He MC, Zhang GF, Qi G, Li Q, Jia QZ, Zhou J (2007) Stability control of surrounding rocks in deep entry of Jiahe coal mine. J Min Saf Eng (China) 24(1):27–30

He MC, Gao YB, Yang J, Gong WL (2017a) An innovative approach for gob-side entry retaining in thick coal seam longwall mining. Energies 10(11):1785–1807

He MC, Gao YB, Yang J, Guo ZB, Wang EY, Wang YJ (2017b) An energy-gathered roof cutting technique in no-pillar mining and its impact on stress variation in surrounding rocks. China J Rock Mech Eng (China) 36(6):1314–1325

He MC, Wang YJ, Yang J, Zhou P, Gao Q, Gao YB (2018) Comparative analysis on stress field distributions in roof cutting nonpillar mining method and conventional mining method. J China Coal Soc 43(3): 626–637

Huang BX, Liu JW, Zhang Q (2018) The reasonable breaking location of overhanging hard roof for directional hydraulic fracturing to control strong strata behaviors of gob-side entry. Int J Rock Mech Min Sci 103:1–11

Itasca Cons (2014) Itasca Consulting Group Inc., UDEC code-version 6. Minneapolis-Minnesota

Kang HP, Lou JF, Gao FQ, Yang JH, Li JZ (2018) A physical and numerical investigation of sudden massive roof collapse during longwall coal retreat mining. Int J Coal Geol 188:25–36

Li M, Zhou N, Zhang JX, Liu ZC (2017) Numerical modelling of mechanical behavior of coal mining hard roofs in different backfill ratios: a case study. Energies 10(7):1005–1023

Li JZ, Zhang M, Li Y, Hu H (2018) Surrounding rock control mechanism in the gob-side retaining entry in thin coal seams, and its application. J S Afr Inst Min Metall 118(5):471–480

Liu XS, Ning JG, Tan YL, Xu Q, Fan DY (2018) Coordinated supporting method of gob-side entry retaining in coal mines and a case study with hard roof. Geomech Eng 15(6):1173–1182

Lu CP, Liu GJ, Liu Y, Zhang N, Xue JH, Zhang L (2015) Microseismic multi-parameter characteristics of rockburst hazard induced by hard roof fall and high stress concentration. Int J Rock Mech Min Sci 76: 18–32

Luan H, Jiang Y, Zhou L, Lin HL (2018) Stability control and quick retaining technology of gob-side entry: a case study. Adv Civ Eng 2018:1–13

Luo Y (2012) Experimental study on supporting technology of gob-side entry with different roof conditions. J Coal Sci Eng (China) 18:238–246

Meguid MA, Saada O, Nunes MA, Mattar J (2008) Physical modeling of tunnels in soft ground: a review. Tunn Undergr Space Technol 23(2):185–198

Ning JG, Liu XS, Tan J, Gu QH, Tan YL, Wang JQ (2018) Control mechanisms and design for a 'coal-backfill-gangue' support system for coal mine gob-side entry retaining. Int J Oil Gas Coal T 18(3/4): 444–466

Roest A, Hart D, Lorig LJ (1990) Modelling fault-slip in underground mining with the distinct element method. Proceedings of the Sixth International Congress of the International Association of Engineering Geology, Amsterdam, Holland, pp 105–110

Sitharam TG, Latha GM (2002) Simulation of excavations in jointed rock masses using a practical equivalent continuum approach. Int Rock Mech Min Sci 39(4):517–525

Sun XM, Liu X, L GF, Wang D, Jiang YL (2014) Key parameters of gob-side entry retaining formed by roof cut and pressure releasing in thin coal seams. Chin J Rock Mech Eng (China) 33(7):1449–1456

Sun XM, Chen F, He MC, Gong WL, Xu HC, Lu H (2017) Physical modeling of floor heave for the deepburied roadway excavated in ten degree inclined strata using infrared thermal imaging technology. Tunn Undergr Space Technol 63:228–243

Sun XM, Chen F, Miao CY, Song P, Li G, Zhao CW, Xia X (2018a) Physical modeling of deformation failure mechanism of surrounding rocks for the deep-buried tunnel in soft rock strata during the excavation. Tunn Undergr Space Technol 74:247–261

Sun XM, Li G, Song P, Miao CY, Zhao CW, Li Q, Xia X (2018b) Application research on gob-side entry retaining methods in no. 1200 working face in Zhongxing mine. Geotech Geologic Eng 37: 185–200

Tan YL, Yu FH, Ning JG, Zhao TB (2015) Design and construction of entry retaining wall along a gob side under hard roof stratum. Int J Rock Mech Min Sci 77:115–121

Tao ZG, Song ZG, He MC, Meng ZG, Pang SH (2018) Principles of the roof cut short-arm beam mining method (110 method) and its mining-induced stress distribution. Int J Min Sci Technol 28(3): 391–396

Tian QY, Zhang JT, Zhang YL (2018) Similar simulation experiment of expressway tunnel in karst area. Constr Build Mater 176:1–13

Wang DC, Li SC, W Q, Li WT, Wang FQ, Wang HT, Peng P, Ruan GQ (2014) Experimental study of reasonable coal pillar width in fully mechanized top coal caving face of deep thick coal seam. Chin J Rock Mech Eng (China) 33(3):539–548

Wang Q, Gao HK, Jiang B, Li S, He MC, Wang DC, Lu W, Qin Q, Gao S, Yu HC (2017) Research on reasonable coal pillar width of roadway driven along goaf in deep mine. Arab J Geosci 10(21):466–483

Wang YJ, Gao YB, Wang EY, He MC, Yang J (2018a) Roof deformation characteristics and preventive techniques using a novel non-pillar mining method of gob-side entry retaining by roof cutting. Energies 11(3):627–644

Wang Q, He MC, Yang J, Gao HK, Jiang B, Yu HC (2018b) Study of a no-pillar mining technique with automatically formed gob-side entry retaining for longwall mining in coal mines. Int J Rock Mech Min Sci 110:1–8

Wang YJ, He MC, Zhang KX, Yang J, Zhen EZ, Zhu Z, Gao YB, Ma ZM (2018c) Strata behavior characteristics and control countermeasures for the gateroad surroundings in innovative non-pillar mining method with gateroad formed automatically. J Mining Safety Eng (China) 4(3):677–685

Wang YJ, He MC, Yang J, Wang Q, Liu JN, Tian XC, Gao YB (2020a) Case study on pressure-relief mining technology without advance tunneling and coal pillars in longwall mining. Tunn Undergr Space Technol 97:103236.1–103236.13

Wang Q, Jiang ZH, Jiang B, Gao HK, Huang YB, Zhang P (2020b) Research on an automatic roadway formation method in deep mining areas by roof cutting with high-strength bolt-grouting. Int J Rock Mech Min Sci 128:104264–104277

Wu LX, Qian MG, Wang JZ (1997) The influence of a thick hard rock stratum on underground mining subsidence. Int J Rock Mech Min Sci 34(2):341–344

Xie PS, Luo Y, Wu YP, Gao XC, Luo SH, Zeng YF (2020) Roof deformation associated with mining of two panels in steeply dipping coal seam using subsurface subsidence prediction model and physical simulation experiment. Min Metall Explor 37(10):581–591

Xue DP, Wang JP, Tu HS, Wang FT, Zhao J (2013) Deformation failure mechanism and application of the backfill along the goaf-side retained roadway. Int J Min Sci Technol 23(3):329–335

Yan S, Liu TX, Bai JB (2018) Key parameters of gob-side entry retaining in a gassy and thin coal seam with hard roof. Processes 6(5):51–65

Yang J, He MC, Cao C (2019) Design principles and key technologies of gob side entry retaining by roof pre-fracturing. Tunn Undergr Space Technol 90:309–318

Yang XJ, Mao WB, Wang EY, Sun Y, Wang JM, He MC (2020) Mechanism and control methods of roof deformations in gob-side entry retention by roof cutting under medium-thick coal seams. Geotech Geol Eng 38(4):265–282

Zhang GF, He MC, Yu XP, Huang ZG (2011) Research on the technique of no-pillar mining with gob-side entry formed by advanced roof caving in the protective seam in Baijiao coal mine. J Mining Safety Eng (China) 28(4):511–516

Zhang N, Yuan L, Han CL, Xue JH, Kan JG et al (2012) Stability and deformation of surrounding rock in pillar less gob-side entry retaining. Saf Sci 50(4):593–599

Zhang YQ, Tang JX, Xiao DQ, Sun LL, Zhang WZ (2014) Spontaneous caving and gob-side entry retaining of thin seam with large inclined angle. Int J Min Sci Technol 24(4):441–445

Zhang GF, Xu YQ, Ge PT (2016) Research on cut gob-side entry retaining in thin coal seam of Tangshan ditch. Chin J Rock Mech Eng (China) 35(7):1397–1406

Zhang ZY, Shimada H, Sasaoka T, Hamanaka A (2017) Stability control of retained goaf-side gateroad under different roof conditions in deep underground Y type longwall mining. Sustainability 9(10): 1671–1690

Zhang ZZ, Wang WJ, Li SQ, Bai JB, Hao SQ, Wu H, Yu XY (2018) An innovative approach for gob-side entry retaining with thick and hard roof: a case study. Teh Vjesn 25(4):1028–1036

Zhao T, Liu CY, Yetilmezsoy K, Zhang BS, Zhang S (2017) Fractural structure of thick hard roof stratum using long beam theory and numerical modeling. Environ Earth Sci 76(21):751–764

Zhao PX, Zhuo RS, Li SG, Ho CH, Lin HF, Liu H (2019) Research on the effect of coal seam inclination on gas migration channels at fully mechanized coal mining face. Arab J Geosci 12(18):1–14